Supercomputer Modeling of Wave Propagation in Blocky Media Accounting Fractures of Interlayers

Vladimir M. Sadovskii, Oxana V. Sadovskaya

Institute of Computational Modeling SB RAS, Krasnoyarsk, Russia
Department of Computational Mechanics of Deformable Media

sadov@icm.krasn.ru, o_sadov@icm.krasn.ru

UNIVERSITÀ DEGLI STUDI DELL'AQUILA
M&MOCS
International Research Center on
MATHEMATICS AND MECHANICS
OF COMPLEX SYSTEMS

ROMA TRE
UNIVERSITÀ DEGLI STUDI

International Conference
on Nonlinear Solid Mechanics

ICoNSoM 2019

16 – 19 June 2019
Roma, Italy

Contents

A blocky model of geological media

The faults and/or filed fractures in the reservoir introduce a network, communicate hydraulically between each other locally and globally, and provide overall conductivity (permeability) of the reservoir, and the matrix provides overall storage capacity (porosity).

Dual-porosity reservoir model

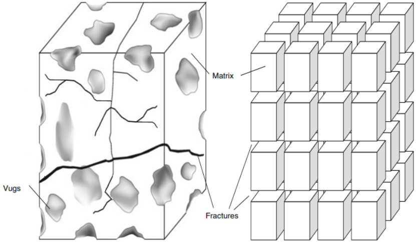

Fractured reservoir   Sugar cube representation

Warren J.E., Root P.J. **The behavior of naturally fractured reservoirs. SPE J.** 1963. V. 3. P. 245–255.

Sadovskii M.A. **Natural lumpiness of a rock. Dokl. Akad. Nauk SSSR**. 1979. V. 247, No. 4. P. 829–831.

Elastic blocks and elastic interlayers

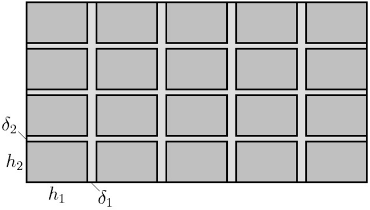

Scheme of a blocky medium

A motion of each block is defined by the system of equations of a homogeneous isotropic elastic medium:

$$\rho\,\dot v_1 = \sigma_{11,1} + \sigma_{12,2}$$
$$\rho\,\dot v_2 = \sigma_{12,1} + \sigma_{22,2}$$
$$\dot\sigma_{11} = \rho\,c_1^2\big(v_{1,1} + v_{2,2}\big) - 2\,\rho\,c_2^2\,v_{2,2}$$
$$\dot\sigma_{22} = \rho\,c_1^2\big(v_{1,1} + v_{2,2}\big) - 2\,\rho\,c_2^2\,v_{1,1}$$
$$\dot\sigma_{12} = \rho\,c_2^2\big(v_{2,1} + v_{1,2}\big)$$

Elastic interlayer between the horizontally located nearby blocks is described by the system of equations:

$$\rho'\,\frac{\dot v_1^+ + \dot v_1^-}{2} = \frac{\sigma_{11}^+ - \sigma_{11}^-}{\delta_1}, \qquad \frac{\dot\sigma_{11}^+ + \dot\sigma_{11}^-}{2} = \rho'\,{c_1'}^2\,\frac{v_1^+ - v_1^-}{\delta_1}$$
$$\rho'\,\frac{\dot v_2^+ + \dot v_2^-}{2} = \frac{\sigma_{12}^+ - \sigma_{12}^-}{\delta_1}, \qquad \frac{\dot\sigma_{12}^+ + \dot\sigma_{12}^-}{2} = \rho'\,{c_2'}^2\,\frac{v_2^+ - v_2^-}{\delta_1}$$

Elastic interlayer between the vertically located nearby blocks is modeled using similar system:

$$\rho'\,\frac{\dot v_2^+ + \dot v_2^-}{2} = \frac{\sigma_{22}^+ - \sigma_{22}^-}{\delta_2}, \qquad \frac{\dot\sigma_{22}^+ + \dot\sigma_{22}^-}{2} = \rho'\,{c_1'}^2\,\frac{v_2^+ - v_2^-}{\delta_2}$$
$$\rho'\,\frac{\dot v_1^+ + \dot v_1^-}{2} = \frac{\sigma_{12}^+ - \sigma_{12}^-}{\delta_2}, \qquad \frac{\dot\sigma_{12}^+ + \dot\sigma_{12}^-}{2} = \rho'\,{c_2'}^2\,\frac{v_1^+ - v_1^-}{\delta_2}$$

Elastic–plastic interlayers

To take into account the plasticity, constitutive equations of the vertical elastic interlayer are replaced by the variational inequality:

$$(\delta\sigma_{11}^{+} + \delta\sigma_{11}^{-})\,\dot\varepsilon_{11}^{p} + (\delta\sigma_{12}^{+} + \delta\sigma_{12}^{-})\,\dot\varepsilon_{12}^{p} \leqslant 0$$

$\delta\sigma_{jk}^{\pm} = \tilde\sigma_{jk}^{\pm} - \sigma_{jk}^{\pm}$ – variations of stresses

$\dot\varepsilon_{11}^{p} = \dfrac{v_1^{+} - v_1^{-}}{\delta_1} - \dfrac{\dot\sigma_{11}^{+} + \dot\sigma_{11}^{-}}{2\,\rho' {c'_1}^2}, \quad \dot\varepsilon_{12}^{p} = \dfrac{v_2^{+} - v_2^{-}}{\delta_1} - \dfrac{\dot\sigma_{12}^{+} + \dot\sigma_{12}^{-}}{2\,\rho' {c'_2}^2}$ – plastic strain rates

The actual stresses $\sigma_{jk}^{\pm}$ and variable stresses $\tilde\sigma_{jk}^{\pm}$ are subjected to the constraint in the form:

$$f\left(\frac{\tilde\sigma_{11}^{+} + \tilde\sigma_{11}^{-}}{2}, \frac{\tilde\sigma_{12}^{+} + \tilde\sigma_{12}^{-}}{2}\right) \leqslant \tau(\chi)$$

τ – material yield point of interlayers, χ – material parameter (or set of parameters) of hardening
$f(\sigma_n, \sigma_\tau)$ – equivalent stress function, in which arguments are normal and tangential stresses

The simplest form of the constraint for a microfractured medium is as follows:

$$|\sigma_\tau| \leqslant \tau_s - k_s\,\sigma_n \qquad (\tau_s \text{ and } k_s \text{ – material parameters})$$

Constitutive equations of the horizontal elastic–plastic interlayer are formulated in a similar way

Poynting–Thomson's viscoelastic model

To describe the viscous dissipative effects in the interlayers under shear stresses, the Poynting–Thomson model of a viscoelastic medium is used.

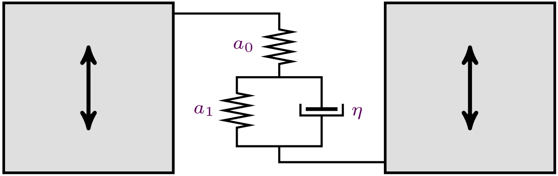

Poynting–Thomson's rheological scheme

Hooke's law for elastic element: $\varepsilon'_{12} = a_0\,(\sigma^+_{12} + \sigma^-_{12})/2, \quad \varepsilon''_{12} = a_1 s_{12}$

Newton's law for viscous element: $\eta\,\dot\varepsilon''_{12} = (\sigma^+_{12} + \sigma^-_{12})/2 - s_{12}$ Total strain: $\varepsilon_{12} = \varepsilon'_{12} + \varepsilon''_{12}$

Constitutive equations of the interlayer:

$$a_0\,\frac{\dot\sigma^+_{12} + \dot\sigma^-_{12}}{2} + a_1\,\dot s_{12} = \frac{v^+_2 - v^-_2}{\delta_1}, \qquad \frac{\sigma^+_{12} + \sigma^-_{12}}{2} = s_{12} + \eta\,a_1\,\dot s_{12}$$

Energy balance equation:

$$\frac{\sigma^+_{12} + \sigma^-_{12}}{2}\,\frac{v^+_2 - v^-_2}{\delta_1} = \dot W + \eta\,a_1^2\,\dot s_{12}^2, \quad 2\,W = a_0\,\frac{(\sigma^+_{12} + \sigma^-_{12})^2}{4} + a_1\,s_{12}^2$$

according to which the power of internal stresses in the interlayer is the sum of the reversible elastic strain power and the power of the viscous energy dissipation

Model of porous interlayers

The longitudinal deformation of the interlayers is described on the basis of a complicated version of the porous elastic model, which takes into account the strength increasing during the collapse of pores.

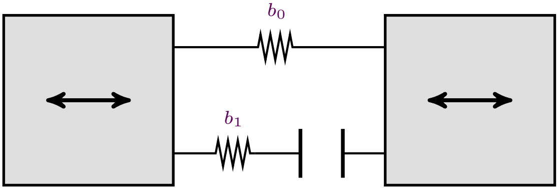

Rheological scheme of a porous interlayer

Total strain: $\varepsilon_{11} = \sigma'_{11}/b_1 + \theta_1 - \theta_0$

$\sigma'_{11} \leqslant 0$ – stress in a rigid contact, $\theta_0 > 0$ and $\theta_1 \geqslant 0$ – initial and current porosity values

Governing relationships of a rigid contact: $(\tilde{\sigma}_{11} - \sigma'_{11})\,\theta_1 \leqslant 0, \quad \tilde{\sigma}_{11},\, \sigma'_{11} \leqslant 0$

$\sigma'_{11} = b_1\,\pi(\theta_0 + \varepsilon_{11}), \ \pi(\theta) = \min(\theta, 0)$ – projection onto the non-positive semi-axis

Constitutive equations of the interlayer including the equation for porosity:

$$\dot{\varepsilon}_{11} = \frac{v_1^+ - v_1^-}{\delta_1}, \quad \frac{\sigma_{11}^+ + \sigma_{11}^-}{2} = b_0\,\varepsilon_{11} + b_1\,\pi(\theta_0 + \varepsilon_{11}), \quad \theta_1 = \theta_0 + \varepsilon_{11} - \pi(\theta_0 + \varepsilon_{11})$$

The energy balance equation: $\dfrac{\sigma_{11}^+ + \sigma_{11}^-}{2}\,\dot{\varepsilon}_{11} = \dot{W}, \quad 2\,W = b_0\,\varepsilon_{11}^2 + b_1\,\pi^2(\theta_0 + \varepsilon_{11})$

Modified Biot's model

For fluid-saturated porous interlayers, a version of the model is applied based on Biot's approach.

Kinetic energy related to the initial unit of a volume of the horizontal interlayers:

$$2\,T = \rho_s\,\frac{(v_1^+ + v_1^-)^2}{4} + \rho_a\Bigl(\frac{v_1^+ + v_1^-}{2} - w_1\Bigr)^2 + (\rho_s + \rho_f)\,\frac{(v_2^+ + v_2^-)^2}{4} + \rho_f\,w_1^2$$

ρ_s and ρ_f – partial densities of a solid skeleton and a liquid phase in interlayers
ρ_a – density of additional mass, w_1 – absolute velocity of a fluid

Equations describing skeleton motion in the direction of longitudinal axis x_1:

$$(\rho_s + \rho_a)\,\frac{\dot v_1^+ + \dot v_1^-}{2} - \rho_a\,\dot w_1 = \frac{\sigma_{12}^+ - \sigma_{12}^-}{\delta_2}$$

$$a_0\,\frac{\dot\sigma_{12}^+ + \dot\sigma_{12}^-}{2} + a_1\,\dot s_{12} = \frac{v_1^+ - v_1^-}{\delta_2}, \qquad \frac{\sigma_{12}^+ + \sigma_{12}^-}{2} = s_{12} + \eta\,a_1\,\dot s_{12}$$

Equations describing joint motion of the solid and liquid phase in the direction of transverse axis x_2:

$$(\rho_s + \rho_f)\,\frac{\dot v_2^+ + \dot v_2^-}{2} = \frac{\sigma_{22}^+ - \sigma_{22}^-}{\delta_2}, \quad \dot\varepsilon_{22} = \frac{v_2^+ - v_2^-}{\delta_2}, \quad \frac{\dot\sigma_{22}^+ + \dot\sigma_{22}^-}{2} = b_0\,\dot\varepsilon_{22} + b_1\,\dot\pi(\theta_0 + \varepsilon_{22}) + b_s\,w_{1,1}$$

Equations describing the fluid motion along the interlayer:

$$(\rho_f + \rho_a)\,\dot w_1 - \rho_a\,\frac{\dot v_1^+ + \dot v_1^-}{2} = s_{11,1}, \quad \dot s_{11} = b_f\,w_{1,1} + b_s\,\dot\varepsilon_{22}$$

$s_{11} = -p\,\theta$ – normal stress in liquid phase, p – pore pressure, θ – momentary porosity
b_s and b_f – elastic moduli in the system "solid skeleton–fluid"

Kirchhoff's law for nodes

The computational algorithm based on the Godunov gap decay scheme is applied at the stage of approximation of the equations for velocity w_1 and stress s_{11} in a fluid.

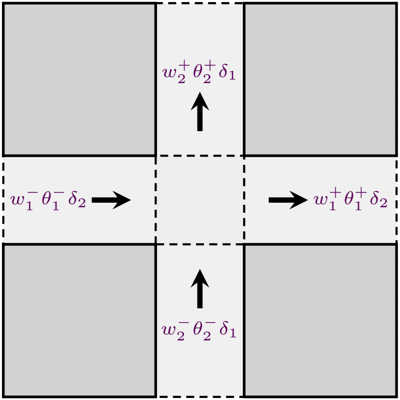

Scheme of flows interaction

At junction zones of the horizontal and vertical interlayers, the internal boundary conditions are set.

They result from Kirchhoff's law for the fluid flow:

$$w_1^+\,\theta_1^+\,\delta_2 + w_2^+\,\theta_2^+\,\delta_1 = w_1^-\,\theta_1^-\,\delta_2 + w_2^-\,\theta_2^-\,\delta_1$$

and the dynamic equations:

$$s_{11}^{\pm} = -p\,\theta_1^{\pm}, \quad s_{22}^{\pm} = -p\,\theta_2^{\pm}$$

considering the pressure equality at a junction.

$\theta_1^{\pm}$ and $\theta_2^{\pm}$ – porosities in the horizontal and vertical interlayers

In this formulation of the boundary conditions at the junctions, the power balance equation is fulfilled:

$$s_{11}^+\,w_1^+\,\delta_2 + s_{22}^+\,w_2^+\,\delta_1 - s_{11}^-\,w_1^-\,\delta_2 - s_{22}^-\,w_2^-\,\delta_1 = 0$$

which guarantees the thermodynamic consistency of equations in the inner layers and blocks.

Model of separation cracks

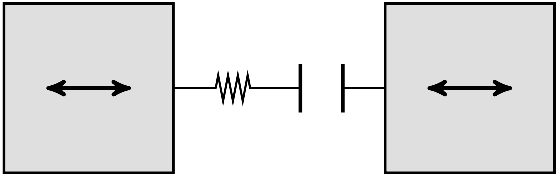

Rheological scheme of contact interaction of crack edges

Conditions of contact interaction of the crack edges are formulated as a variational inequality

$$\delta\sigma_{11}\left(\frac{1}{\rho' c_1'^2}\,\sigma_{11}-\varepsilon_{11}\right)\geqslant 0,\qquad \dot{\varepsilon}_{11}=\frac{v_1^+-v_1^-}{\delta_1}$$

The algorithm of numerical implementation in a mesh of grid is based on the equations

$$\hat{\varepsilon}_{11}=\varepsilon_{11}+\frac{v_1^+-v_1^-}{\delta_1}\,\tau,\qquad z_1v_1^+ +\sigma_{11}^+=R_1^+,\qquad z_1v_1^- -\sigma_{11}^-=R_1^-$$

and the closing equation $\hat{\sigma}_{11}+\sigma_{11}=\sigma_{11}^+ +\sigma_{11}^-$, guaranteeing the absence of artificial dissipation of energy, which gives the procedure of stress correction

$$\hat{\sigma}_{11}=\frac{1}{\kappa}\,\pi_-\left(\varepsilon_{11}+\frac{R_1^+-R_1^- -\sigma_{11}}{z_1\delta_1}\,\tau\right),\qquad \kappa=\frac{1}{\rho' c_1'^2}+\frac{\tau}{\rho\, c_1\delta_1}$$

Two-cyclic splitting

We developed parallel computational algorithm for supercomputers of the cluster architecture based on a two-cyclic method of splitting, which permits the efficient parallelization of computations.

Governing equations in blocks and interlayers are represented in the form of symbolic evolution equation:

$$\dot{U} = A_1(U) + A_2(U)$$

A_1 and A_2 – nonlinear differential-difference operators, simulating 1D motion of a blocky medium in the direction of the coordinate axes x_1 and x_2, U – vector–function of unknown quantities which includes the projection of the velocity vector and the stress tensor in blocks and interlayers

The method of splitting on the time interval $(t_0, t_0 + \Delta t)$ includes four steps: the step of solving 1D equation in the x_1 direction on the interval $(t_0, t_0 + \Delta t/2)$, a similar step of solving the equation in the x_2 direction, the step of recomputation in the x_2 direction on the interval $(t_0 + \Delta t/2, t_0 + \Delta t)$ and the step of recomputation in the x_1 direction on the same interval:

$$\begin{aligned}
\dot{U}^{(1)} &= A_1(U^{(1)}), \quad U^{(1)}(t_0) = U(t_0) \\
\dot{U}^{(2)} &= A_2(U^{(2)}), \quad U^{(2)}(t_0) = U^{(1)}(t_0 + \Delta t/2) \\
\dot{U}^{(3)} &= A_2(U^{(3)}), \quad U^{(3)}(t_0 + \Delta t/2) = U^{(2)}(t_0 + \Delta t/2) \\
\dot{U}^{(4)} &= A_1(U^{(4)}), \quad U^{(4)}(t_0 + \Delta t/2) = U^{(3)}(t_0 + \Delta t)
\end{aligned}$$

The solution at the time instant $t_0 + \Delta t$ equals to $U(t_0 + \Delta t) = U^{(4)}(t_0 + \Delta t)$

Efficiency of parallelization

Computational algorithm is implemented as the parallel program. Parallelization is performed on the basis of domain decomposition – each processor of a cluster expects a separate chain of blocks including the boundary interlayers in the horizontal direction.

The programming language is Fortran, and the message passing interface (MPI) library is used.

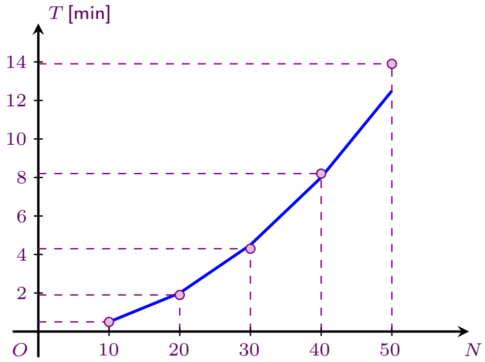

Dependence of the runtime T on the linear dimension N of a grid in blocks
(circle points – actual computational time, solid line – semi-theoretical computational time)

Instant rotation of the central block in the rock mass

$\delta = 0.1$ mm $\qquad \delta = 1$ mm $\qquad \delta = 5$ mm

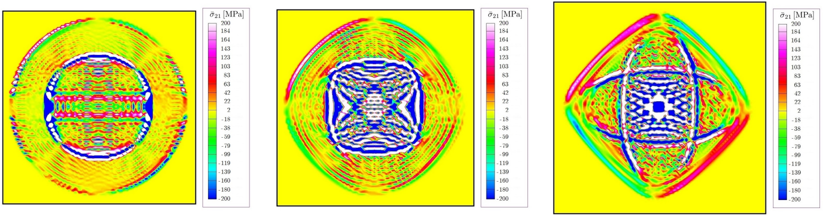

Level curves of the tangential stress depending on the thickness of interlayers

The case of porous interlayers

Rock massif consists of 100 × 100 blocks, size of each block is 50 mm × 50 mm

Sadovskii V.M., Sadovskaya O.V. **Modeling of elastic waves in a blocky medium based on equations of the Cosserat continuum.** **Wave Motion**. 2015. V. 52. P. 138–150.
DOI: 10.1016/j.wavemoti.2014.09.008
`http://www.sciencedirect.com/science/article/pii/S0165212514001358`

Sadovskii V.M., Sadovskaya O.V., Lukyanov A.A. **Modeling of wave processes in blocky media with porous and fluid-saturated interlayers.** **Journal of Computational Physics**. 2017. V. 345. P. 834–855. DOI: 10.1016/j.jcp.2017.06.001
`http://www.sciencedirect.com/science/article/pii/S0021999117304461`

Instant rotation of the central block in the rock mass

$\delta = 0.1\,\mathrm{mm}$ $\delta = 1\,\mathrm{mm}$ $\delta = 5\,\mathrm{mm}$

The case of elastic interlayers

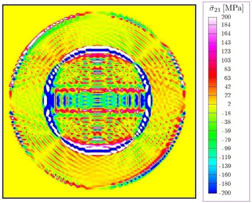

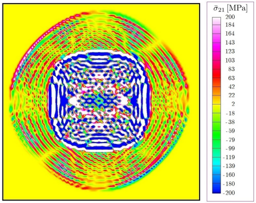

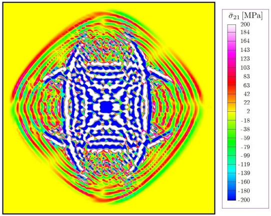

Level curves of the tangential stress depending on the thickness of interlayers

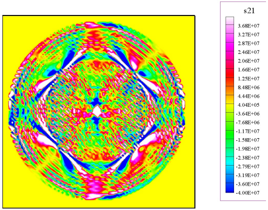

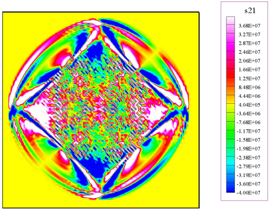

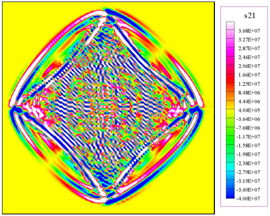

The case of elastic–plastic interlayers

Instant rotation of the central block in the rock mass

$\delta = 0.1\,\text{mm}$ $\qquad$ $\delta = 1\,\text{mm}$ $\qquad$ $\delta = 5\,\text{mm}$

The case of porous interlayers: intensive load (with pore collapse)

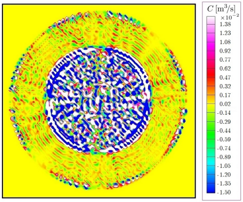

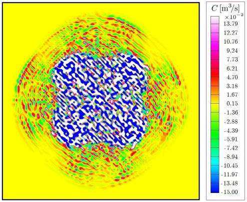

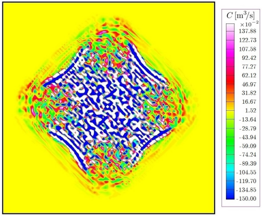

Level curves of the fluid circulation around blocks depending on the thickness of interlayers

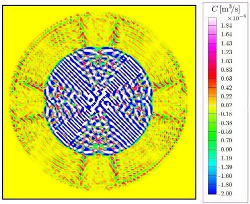

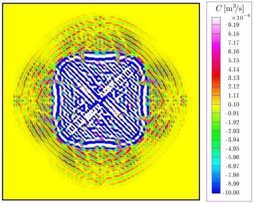

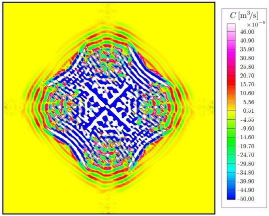

The case of porous interlayers: small load (without pore collapse)

Crack propagation in a blocky medium

The action of Π-shaped pulse load on a part of the upper boundary of a blocky massif

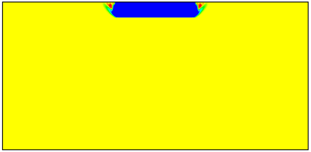

Level curves of the normal stress σ_{22}

Formation and propagation of the system of interblock cracks

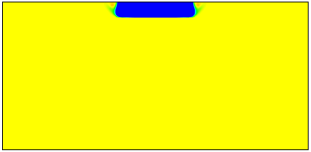

The action of Π-shaped smoothed pulse load on a part of the upper boundary

100 layers, 200 blocks in each of them

100 nodes, 1D decomposition of computational domain

Crack propagation in a blocky medium

The action of Π-shaped pulse load on a part of the upper boundary of a blocky massif

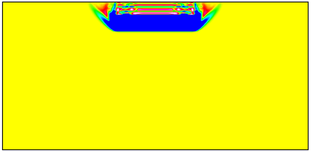

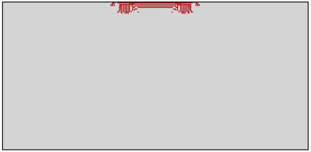

Level curves of the normal stress σ_{22}

Formation and propagation of the system of interblock cracks

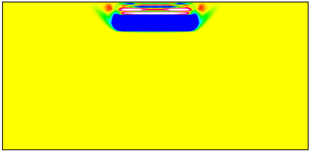

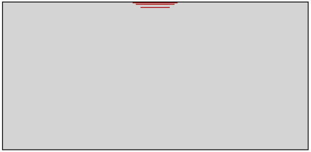

The action of Π-shaped smoothed pulse load on a part of the upper boundary

100 layers, 200 blocks in each of them

100 nodes, 1D decomposition of computational domain

Crack propagation in a blocky medium

The action of Π-shaped pulse load on a part of the upper boundary of a blocky massif

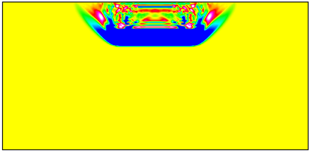

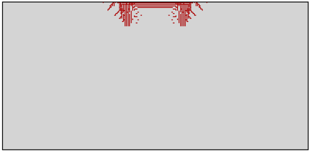

Level curves of the normal stress σ_{22}

Formation and propagation of the system of interblock cracks

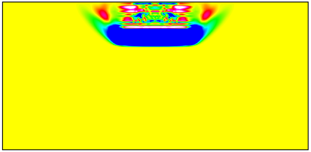

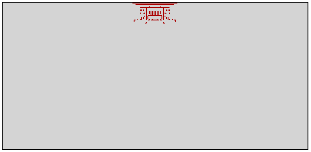

The action of Π-shaped smoothed pulse load on a part of the upper boundary

100 layers, 200 blocks in each of them

100 nodes, 1D decomposition of computational domain

Crack propagation in a blocky medium

The action of Π-shaped pulse load on a part of the upper boundary of a blocky massif

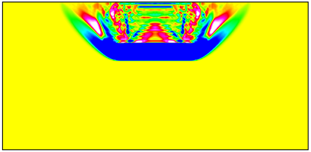

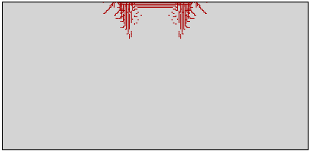

Level curves of the normal stress σ_{22}

Formation and propagation of the system of interblock cracks

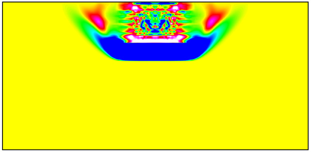

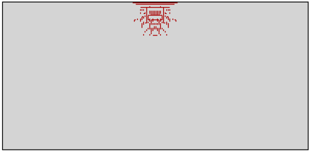

The action of Π-shaped smoothed pulse load on a part of the upper boundary

100 layers, 200 blocks in each of them

100 nodes, 1D decomposition of computational domain

Crack propagation in a blocky medium

The action of Π-shaped pulse load on a part of the upper boundary of a blocky massif

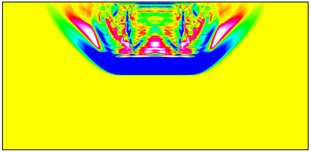

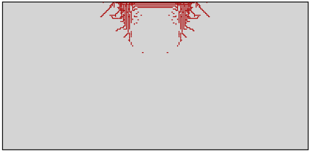

Level curves of the normal stress σ_{22}

Formation and propagation of the system of interblock cracks

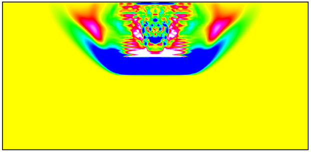

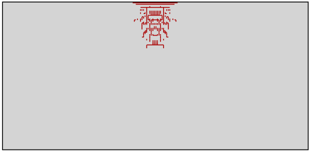

The action of Π-shaped smoothed pulse load on a part of the upper boundary

100 layers, 200 blocks in each of them

100 nodes, 1D decomposition of computational domain

Crack propagation in a blocky medium

The action of Π-shaped pulse load on a part of the upper boundary of a blocky massif

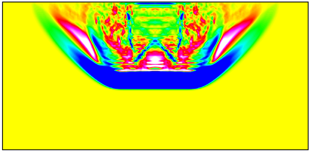

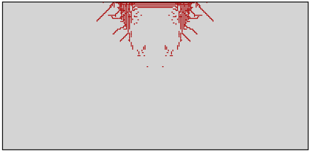

Level curves of the normal stress σ_{22}

Formation and propagation of the system of interblock cracks

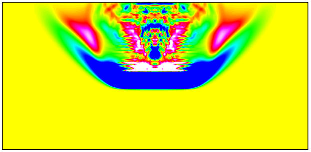

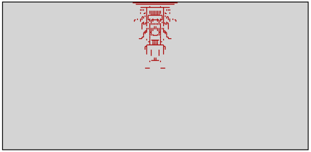

The action of Π-shaped smoothed pulse load on a part of the upper boundary

100 layers, 200 blocks in each of them

100 nodes, 1D decomposition of computational domain

Crack propagation in a blocky medium

The action of Π-shaped pulse load on a part of the upper boundary of a blocky massif

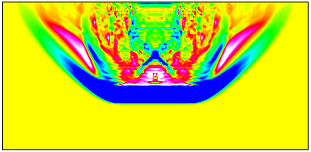

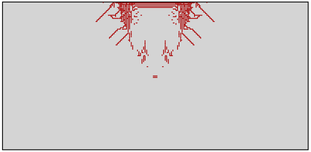

Level curves of the normal stress σ_{22}

Formation and propagation of the system of interblock cracks

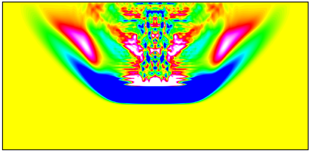

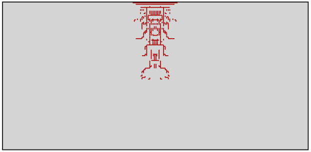

The action of Π-shaped smoothed pulse load on a part of the upper boundary

100 layers, 200 blocks in each of them

100 nodes, 1D decomposition of computational domain

Crack propagation in a blocky medium

The action of Π-shaped pulse load on a part of the upper boundary of a blocky massif

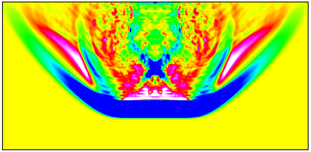

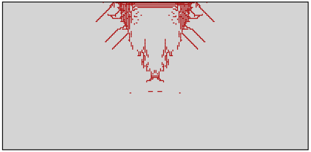

Level curves of the normal stress σ_{22}

Formation and propagation of the system of interblock cracks

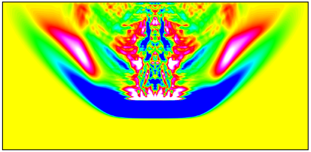

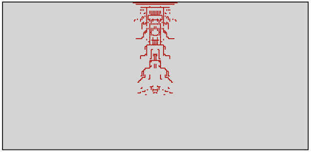

The action of Π-shaped smoothed pulse load on a part of the upper boundary

100 layers, 200 blocks in each of them

100 nodes, 1D decomposition of computational domain

Crack propagation in a blocky medium

The action of Π-shaped pulse load on a part of the upper boundary of a blocky massif

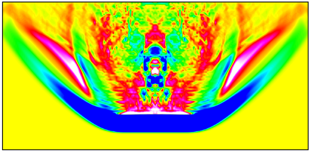

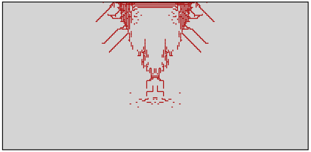

Level curves of the normal stress σ_{22}

Formation and propagation of the system of interblock cracks

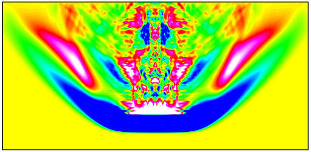

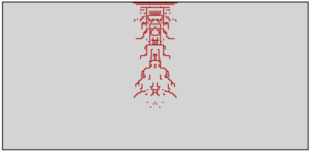

The action of Π-shaped smoothed pulse load on a part of the upper boundary

100 layers, 200 blocks in each of them

100 nodes, 1D decomposition of computational domain

Crack propagation in a blocky medium

The action of Π-shaped pulse load on a part of the upper boundary of a blocky massif

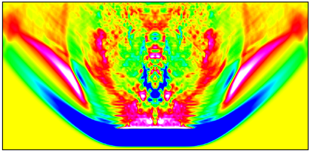

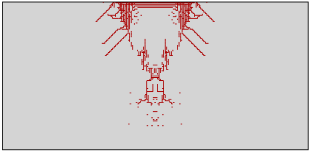

Level curves of the normal stress σ_{22}

Formation and propagation of the system of interblock cracks

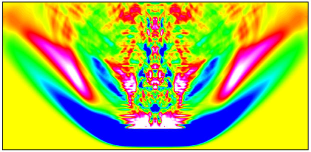

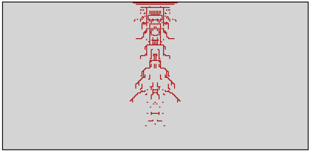

The action of Π-shaped smoothed pulse load on a part of the upper boundary

100 layers, 200 blocks in each of them

100 nodes, 1D decomposition of computational domain

Crack propagation in a blocky medium

The action of Π-shaped pulse load on a part of the upper boundary of a blocky massif

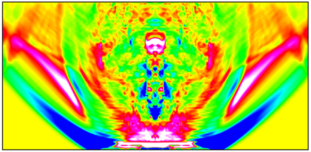

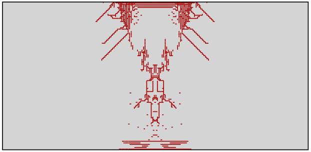

Level curves of the normal stress σ_{22}

Formation and propagation of the system of interblock cracks

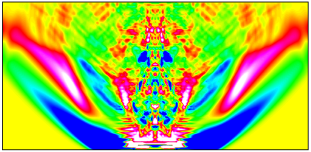

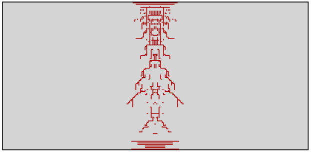

The action of Π-shaped smoothed pulse load on a part of the upper boundary

100 layers, 200 blocks in each of them

100 nodes, 1D decomposition of computational domain

Crack propagation in a blocky medium

The action of Π-shaped pulse load on a part of the upper boundary of a blocky massif

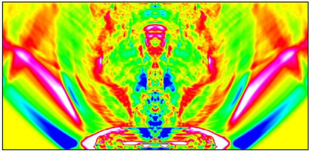

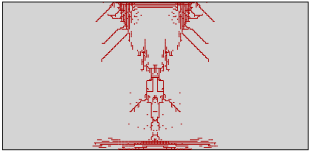

Level curves of the normal stress σ_{22}

Formation and propagation of the system of interblock cracks

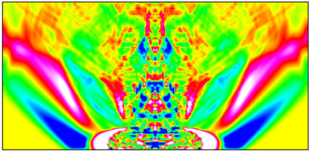

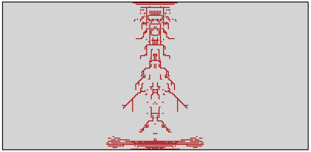

The action of Π-shaped smoothed pulse load on a part of the upper boundary

100 layers, 200 blocks in each of them

100 nodes, 1D decomposition of computational domain

Crack propagation in a blocky medium

The action of Π-shaped pulse load on a part of the upper boundary of a blocky massif

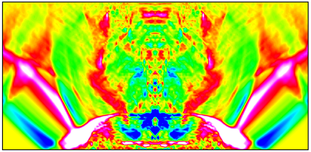

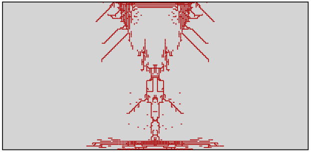

Level curves of the normal stress σ_{22}

Formation and propagation of the system of interblock cracks

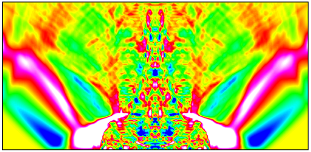

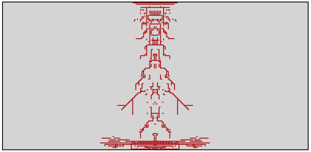

The action of Π-shaped smoothed pulse load on a part of the upper boundary

100 layers, 200 blocks in each of them

100 nodes, 1D decomposition of computational domain

Crack propagation in a blocky medium

The action of Π-shaped pulse load on a part of the upper boundary of a blocky massif

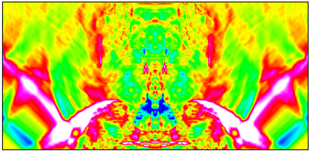

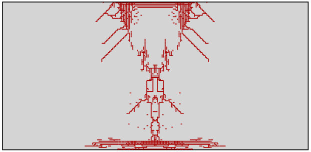

Level curves of the normal stress σ_{22}

Formation and propagation of the system of interblock cracks

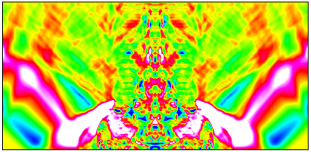

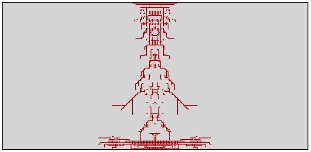

The action of Π-shaped smoothed pulse load on a part of the upper boundary

100 layers, 200 blocks in each of them

100 nodes, 1D decomposition of computational domain

Crack propagation in a blocky medium

The action of Π-shaped pulse load on a part of the upper boundary of a blocky massif

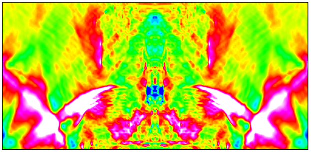

Level curves of the normal stress σ_{22}

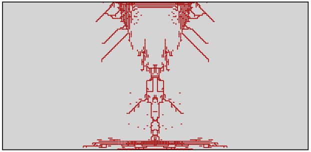

Formation and propagation of the system of interblock cracks

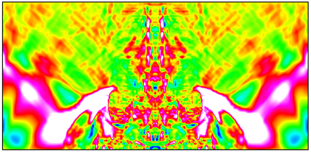

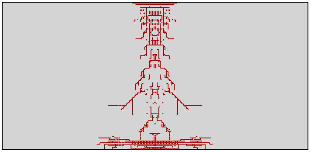

The action of Π-shaped smoothed pulse load on a part of the upper boundary

100 layers, 200 blocks in each of them

100 nodes, 1D decomposition of computational domain

Crack propagation in a blocky medium

The action of Π-shaped pulse load on a part of the upper boundary of a blocky massif

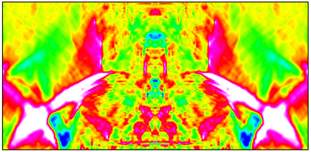

Level curves of the normal stress σ_{22}

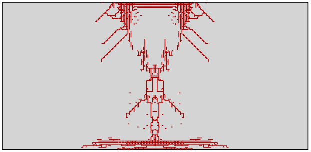

Formation and propagation of the system of interblock cracks

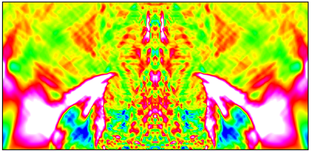

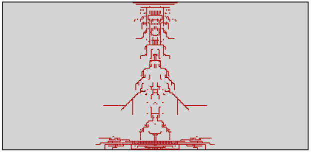

The action of Π-shaped smoothed pulse load on a part of the upper boundary

100 layers, 200 blocks in each of them

100 nodes, 1D decomposition of computational domain

Crack propagation in a blocky medium

The action of Π-shaped pulse load on a part of the upper boundary of a blocky massif

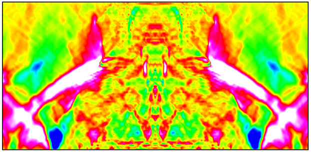

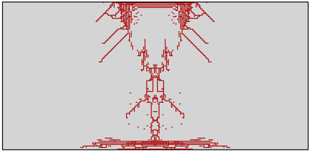

Level curves of the normal stress σ_{22}

Formation and propagation of the system of interblock cracks

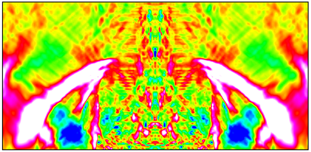

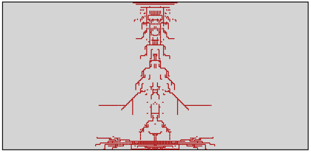

The action of Π-shaped smoothed pulse load on a part of the upper boundary

100 layers, 200 blocks in each of them

100 nodes, 1D decomposition of computational domain

Orthotropic elastic Cosserat continuum

For plane strain, the equations of the Cosserat elastic continuum:

$$\rho_0\,\dot v_1 = \sigma_{11,1} + \sigma_{12,2}, \qquad \rho_0 \dot v_2 = \sigma_{21,1} + \sigma_{22,2}$$

$$J_0\,\dot\omega_3 = \mu_{31,1} + \mu_{32,2} + \sigma_{21} - \sigma_{12}$$

$$a_1\,\dot\sigma_{11} - b_1\,\dot\sigma_{22} = v_{1,1}, \qquad a_1\,\dot\sigma_{22} - b_1\,\dot\sigma_{11} = v_{2,2}$$

$$a_2\,\dot\sigma_{21} - b_2\,\dot\sigma_{12} = v_{2,1} - \omega_3$$

$$a_2\,\dot\sigma_{12} - b_2\,\dot\sigma_{21} = v_{1,2} + \omega_3$$

$$\dot\mu_{31} = \alpha_2\,\omega_{3,1}, \qquad \dot\mu_{32} = \alpha_2\,\omega_{3,2}$$

written in Cartesian coordinates relative to the linear velocities v_1, v_2, angular velocity ω_3, stresses σ_{jk} and couple stresses μ_{jk} can be represented in the matrix form:

$$A\,\frac{\partial U}{\partial t} = B^1\,\frac{\partial U}{\partial x_1} + B^2\,\frac{\partial U}{\partial x_2} + Q\,U$$

$$U = \big(v_1,\, v_2,\, \omega_3,\, \sigma_{11},\, \sigma_{22},\, \sigma_{21},\, \sigma_{12},\, \mu_{31},\, \mu_{32}\big)$$

with symmetric matrix–coefficients A, B^1, B^2 and antisymmetric matrix Q.

This system belongs to the class of symmetric t-hyperbolic systems by Friedrichs and systems of thermodynamically consistent conservation laws by Godunov.

Elastic–plastic Cosserat continuum

It is possible to construct a model of Cosserat elastoplastic continuum on the basis of the system of equations of the theory of elasticity. Such a model is formulated as a variation inequality

$$(\tilde U - U)\cdot\Big(A\,\frac{\partial U}{\partial t} - B^1\,\frac{\partial U}{\partial x_1} - B^2\,\frac{\partial U}{\partial x_2} - Q\,U\Big) \geqslant 0, \qquad \tilde U,\, U \in F$$

F – set of admissible variations of the vector U, $\tilde U$ – arbitrary element of F

This variational inequality is a formulation of the Mises principle of maximum power of plastic dissipation. The boundary of F in the space of stress and couple stress tensors is the yield surface of material, which is equivalent to the system of constitutive equations of plasticity in the form of associative flow role.

Sadovskii V.M. **Discontinuous Solutions in Dynamic Elastic–Plastic Problems.** Physics and Mathematics Literature Publishing Company, Moscow, 1997. 208 p. (in Russian)

Sadovskaya O., Sadovskii V. **Mathematical Modeling in Mechanics of Granular Materials.** Ser.: **Advanced Structured Materials**, Vol. 21. Springer, Heidelberg – New York – Dordrecht – London, 2012. 390 p. DOI: 10.1007/978-3-642-29053-4

http://link.springer.com/book/10.1007/978-3-642-29053-4

Plasticity in interlayers

Since the behavior of continuum is completely determined by the deformation properties of the weakened interlayers of blocky structure, the yield criterion is used in the form:

$$|\sigma_{21}| \leqslant \tau_0 - \kappa_\tau\, \sigma_{11}, \qquad |\sigma_{12}| \leqslant \tau_0 - \kappa_\tau\, \sigma_{22}$$

$$|\mu_{31}| \leqslant \mu_0 - \kappa_\mu\, \sigma_{11}, \qquad |\mu_{32}| \leqslant \mu_0 - \kappa_\mu\, \sigma_{22}$$

It limits the tangential stresses, which characterize shifts along the interlayers, and couple stresses, the attainment of which limit values lead to an irreversible change in the curvature.

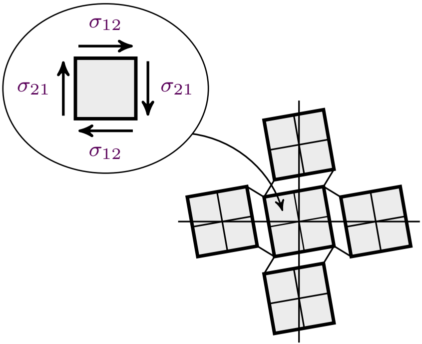

Tangential stresses caused by rotations of the blocks

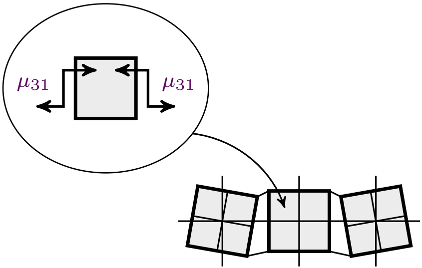

Scheme of couple-stressed interactions

U-shaped pulse loading

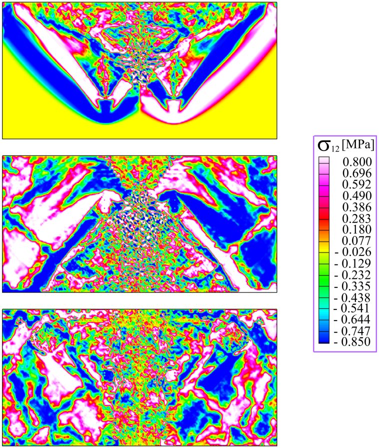

Level curves of tangential stress σ_{12}

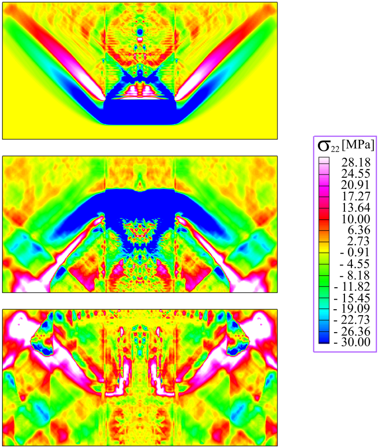

Level curves of normal stress σ_{22}

U-shaped pulse loading

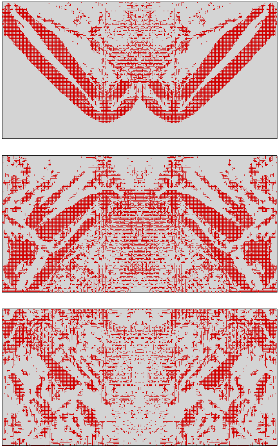

Configuration of plastic zones

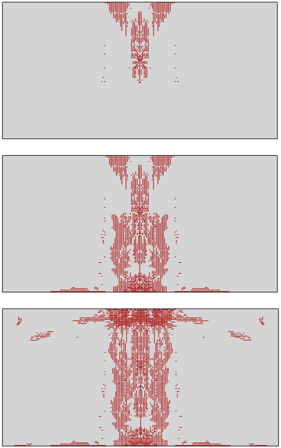

Configuration of fracture zones

Λ-shaped pulse loading

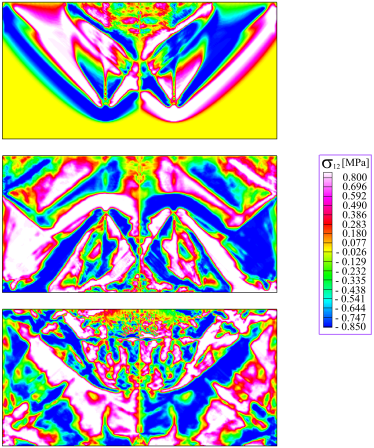

Level curves of tangential stress σ_{12}

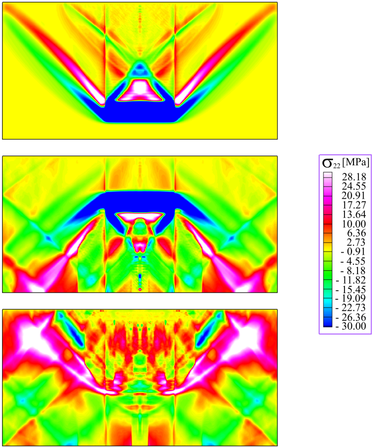

Level curves of normal stress σ_{22}

Λ-shaped pulse loading

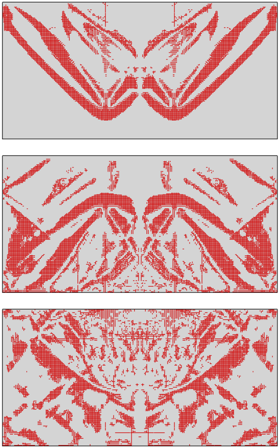

Configuration of plastic zones

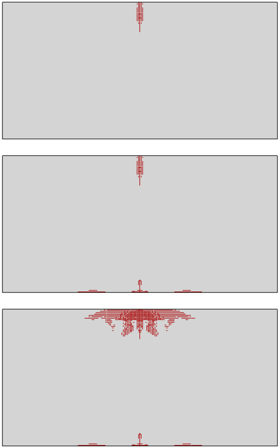

Configuration of fracture zones

U-shaped pulse without fracture

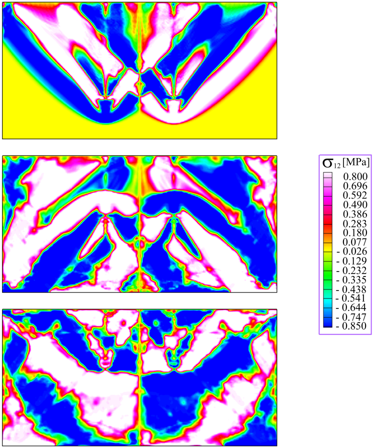

Level curves of tangential stress σ_{12}

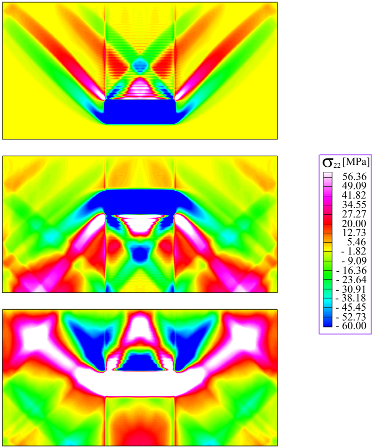

Level curves of normal stress σ_{22}

U-shaped pulse without fracture

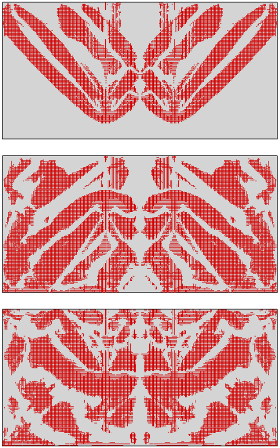

Configuration of plastic zones

U-shaped pulse loading: Cosserat model

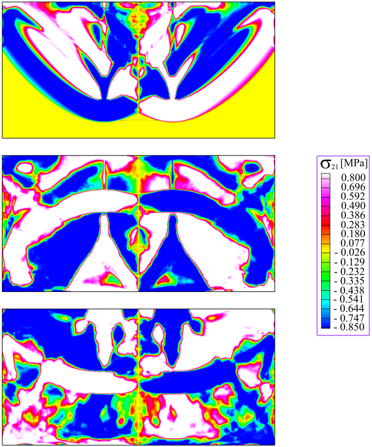

Level curves of tangential stress σ_{21}

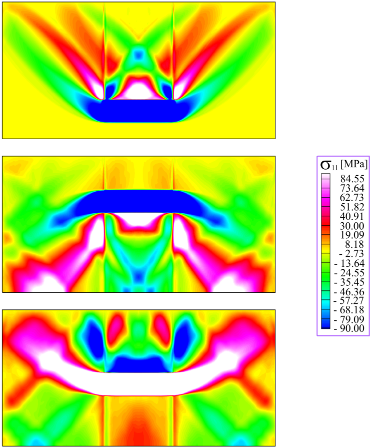

Level curves of normal stress σ_{11}

U-shaped pulse loading: Cosserat model

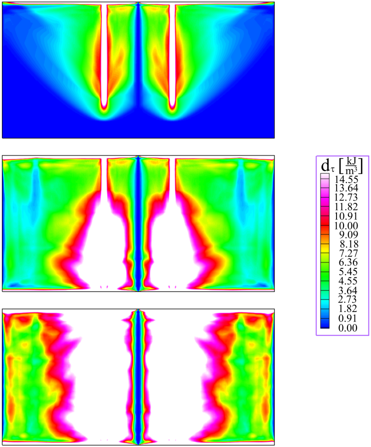

Level curves of plastic dissipative energy

U-shaped pulse loading: Cosserat model

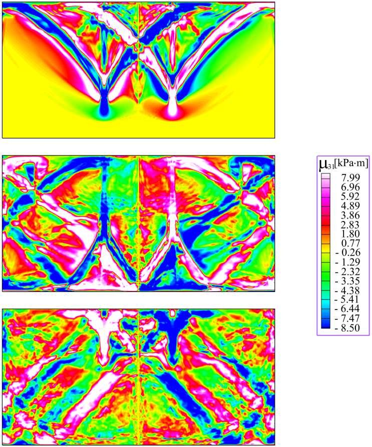

Level curves of couple stress μ_{31}

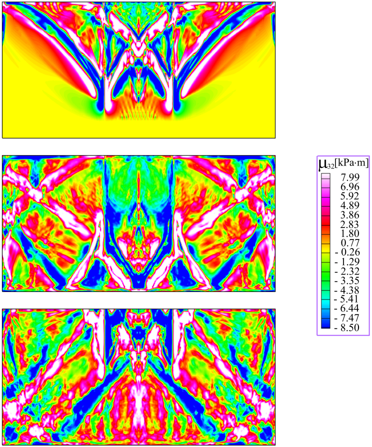

Level curves of couple stress μ_{32}

U-shaped pulse loading: Cosserat model

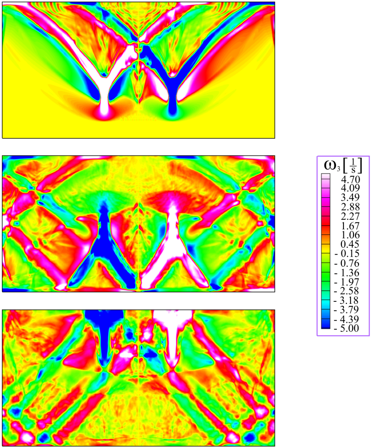

Level curves of angular velocity ω_3

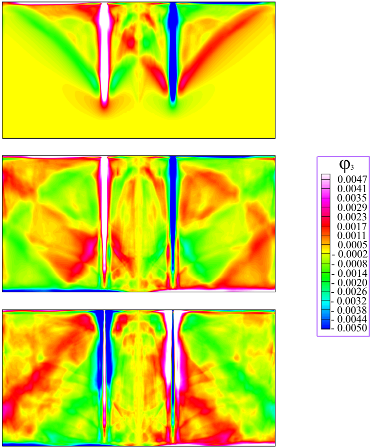

Level curves of rotation angle φ_3 $(\dot{\varphi}_3 = \omega_3)$

Conclusions

- To study wave processes in structurally inhomogeneous media, a discrete-continuous model of a blocky structure composed of elastic blocks is proposed, accounting irreversible deformation, fluid saturation and fracture of weakened interlayers.
- An alternative approach is developed based on the Cosserat model of the orthotropic continuum, taking into account plastic deformation of a material. Comparative analysis showed that by appropriate choosing the mechanical parameters of the Cosserat continuum, it is possible to achieve agreement on the results both on a qualitative and quantitative levels.
- The developed computational algorithms and software can be used to test the adequacy of the formulas for calculating the parameters of the Cosserat continuum of blocky-layered structures obtained as a result of homogenization procedures.

The reported study was funded by the Russian Foundation for Basic Research, Government of Krasnoyarsk Territory, Krasnoyarsk Regional Fund of Science to the research project No. 18-41-242001

Many thanks for your attention and for your interest !!!